RSC Advances

PAPER

View Article Online
View Journal | View Issue

Cite this: *RSC Adv.*, 2020, **10**, 32423

Simplified waste-free process for synthesis of nanoporous compact alumina under technologically advantageous conditions

Alena Fedoročková, *[a] Gabriel Sučik,[a] Beatrice Plešingerová,[a] Ľuboš Popovič,[a] Mária Kovaľaková [b] and Martin Vavra[c]

Precipitated ammonium aluminium carbonate hydroxide ($NH_4Al(OH)_2CO_3$) is a promising precursor for preparation of nanostructured Al_2O_3. However, the experimental conditions, such as the low concentration of Al^{3+} salt solution, high temperature and/or pressure, long reaction time, and excessive amount of the $(NH_4)_2CO_3$ precipitating agent, make this process expensive for large-scale production. Here, we report a simpler and cheaper route to prepare nanostructured alumina by partial neutralisation of a nearly saturated aqueous solution of $Al(NO_3)_3$ with $(NH_4)_2CO_3$ as a base at pH < 4. Synthesis in the acidic region led to formation of a polynuclear aluminium cluster (Al_{13}), which is an important "green" solution precursor for large-area preparation of Al_2O_3 thin films and nanoparticles. Control of the textural properties of the final alumina product during calcination of the prepared aluminium (oxy) hydroxide gel was accomplished by adding low-solubility aluminium acetate hydroxide ($Al(OH)(CH_3COO)_2$) as a seed to the $Al(NO_3)_3$ solution before neutralisation. The large Brunauer–Emmett–Teller specific surface area (376 $m^2\ g^{-1}$) and narrow pore size distribution (2–20 nm) of the prepared compact alumina suggest that the chelating effect of the acetate ions affects the structures of the forming transition aluminas, and the evolved gases produced by decomposition of $Al(OH)(CH_3COO)_2$ and NH_4NO_3 as a by-product of the reaction during calcination prevent particle agglomeration. Other advantages of the proposed process are its versatility and the ability to obtain high purity materials without producing large amounts of by-products without the need for washing and energy saving by using a low processing temperature, and the possibility of recycling the generated CO_2 and NH_3 gases as the $(NH_4)_2CO_3$ reagent.

Received 28th July 2020
Accepted 8th August 2020

DOI: 10.1039/d0ra06544g

rsc.li/rsc-advances

1. Introduction

Alumina (Al_2O_3) is one of the most widely used materials and it has considerable potential in many diverse applications, such as heat insulation,[1] as a catalyst[2–6] and catalyst support,[1,2,4–13] as a high-strength and wear-resistant material in ball mills,[7,8,14] in grinding paste for metal polishing,[8,9] as an inert biomaterial in implants,[15] as a substrate in the electronic industry,[8] in wastewater purification,[3] and in automobile exhaust emission reduction systems and flue gas cleaning.[3,4,6,11,13,16]

The widespread use of Al_2O_3 arises from its high chemical and thermal stability and high mechanical strength, which are predominantly determined by the crystal phase and its composition and structure, mainly the shape and size of the particles and/or pores. In recent years, it has been shown that the performance of alumina in many of the above-mentioned applications can be improved by producing nanoscale structures.[1–3,8–11,17–23] Therefore, current strategies have shifted towards synthesis of aluminium oxide with controllable nanostructure and morphology, because altering the surface area, pore structure, and morphology at the nanoscale can potentially lead to materials with desired physical and chemical properties tailored for various applications.

Several methods have been applied to prepare nanostructured alumina, including gas-phase deposition,[3,14] mechanical grinding,[3] thermal decomposition,[1] combustion methods,[14] microemulsion synthesis,[3,17] the sol–gel process,[1,3,6,8,10,11,14,18,19] precipitation,[3,8,14,21,22] and hydrothermal synthesis.[1,3,8,10,14,21] Among these methods, precipitation is the most popular process for preparation of ultrafine alumina powders because of its simplicity, low cost, safety, and energy and time saving.[3,8,14]

Aluminium hydroxides and (oxo)hydroxides, which are the common precursors to generate Al_2O_3 by thermal treatment, are usually prepared by precipitation of an aluminium salt solution

[a]Faculty of Materials, Metallurgy and Recycling, Technical University of Košice, Letná 9, 042 00 Košice, Slovakia. E-mail: alena.fedorockova@tuke.sk
[b]Faculty of Electrical Engineering and Informatics, Technical University of Košice, Letná 9, 042 00 Košice, Slovakia
[c]Faculty of Science, Pavol Jozef Šafárik University in Košice, Šrobárova 2, 041 54 Košice, Slovakia

with a base such as ammonia.[7,11,14,18,20] It has been demonstrated that bulk precipitation is so rapid that nucleation and growth of particles simultaneously occur, resulting in particles with irregular shapes and a wide size distribution,[7,24] which limit their practical applications.

Recently, synthesis of ammonium aluminium carbonate hydroxide (AACH, $NH_4Al(OH)_2CO_3$) has become a promising alternative for preparation of nanostructured Al_2O_3.[1–3,9,14,20–23] AACH is typically prepared by liquid–liquid precipitation using different aqueous aluminium solutions ($NH_4Al(SO_4)_2$, $Al(NO_3)_3$, $AlCl_3$, and $NaAlO_2$).[3,9,14,20] It has been shown that the choice of an appropriate precipitating agent is crucial for preparation of pure AACH. The product of precipitation using NH_4HCO_3 is a mixture of boehmite (AlO(OH)) and AACH,[14,20] whereas using $(NH_4)_2CO_3$ results in formation of only the AACH phase with low crystallinity.[14] Thus, ammonium carbonate is preferred to ammonium hydrogen carbonate because the latter leads to significant formation of boehmite[20] and the alumina particles prepared using the $(NH_4)_2CO_3$ precipitant show a much narrower distribution and a smaller average diameter than those prepared using NH_4HCO_3.[14] However, precipitation of AACH is very pH sensitive (optimal pH range 9.92–10.28), because AACH can change to AlO(OH) or $[Al(OH)_4]^-$ in concentrated alkaline solution.[3] An alternative novel technique for AACH synthesis that enables control of the morphology of the particles is hydrothermal treatment. Reaction of $Al(NO_3)_3$ aqueous solution or aluminium hydroxide xerogel with a significant stoichiometric excess of ammonium carbonate solution at high temperature and vapour pressure leads to flake-like[2] or rod-like[9] particles.

Thermal treatment after precipitation is accompanied by phase conversion to various aluminium oxide forms. The following sequence has been commonly reported: AlO(OH) → γ-Al_2O_3 → δ-Al_2O_3 → θ-Al_2O_3 → α-Al_2O_3.[8,25] The required temperature for each phase transformation depends on the synthesis method and the specific characteristics of the precursors.[8] For the $NH_4Al(OH)_2CO_3$ precursor, it has been found that transformation to Al_2O_3 does not directly proceed by thermal treatment. During the first step, low crystallinity boehmite (AlO(OH)) is generated. In the second step, boehmite transforms to aluminium oxide with different crystal structures.[9]

Control of the morphology and particle size distribution of the final Al_2O_3 powder can be accomplished by reducing the phase transformation temperature.[7] Various oxides of aluminium, copper, iron, chromium, and magnesium as seeding agents are therefore introduced into the aluminium salt solution before precipitation to act as crystallisation centres to decrease the activation energy of transformation.[25,26] It has been found that the introduced seed particles do not act as nuclei of the new phase, but they affect the structure of the aluminium hydroxide gel formed around them or the structure of the forming transient aluminium oxide.[25]

Although synthesis of nanostructured Al_2O_3 from Al precursors prepared by precipitation has been widely performed, the nanoparticles tended to strongly agglomerate, which caused an increase of the particle size and decreased the specific surface area.[3,14,27] Agglomeration is greatly affected by the aging time of the precipitated precursor.[14] Thus, alumina prepared by precipitation generally exhibits a surface area lower than 300 $m^2\ g^{-1}$.[20] Various approaches have been applied to prevent undesirable aggregation of the nanoparticles during precipitation from solution, as well as during the following drying and thermal treatment, such as addition of organic solvents, surfactants, or chelators.[3,8,11] Even though these dispersants can improve the colloid stability, reduce the temperature required for sintering, enhance green densification, and control the particle morphology,[8] they affect the product crystallinity and are difficult to completely remove from the final materials.[10] In this context, phase transformation of ammonium aluminium carbonate hydroxide to alumina can be helpful to suppress agglomeration, because the CO_2, NH_3, and H_2O gases released during thermal treatment play significant roles in reducing agglomeration of the final Al_2O_3 particles.[14] However, the prepared alumina may have high impurity content owing to insufficient removal of the supernatant solution.[20] Increasing the purity of alumina powder requires a large amount of washing solvent and results in loss of up to 25% of Al_2O_3, as well as generation of solvent waste.[7] Furthermore, excessive washing of AACH ($V_{washing}/V_{suspension} > 1.6$) leads to disappearance of the AACH phase and progressive formation of the boehmite phase.[20]

Since the preparation of monodispersed Al_2O_3 in the published works was carried out with a very low starting concentration of the Al^{3+} solution (≤0.13 M),[1–3,14,21] low productivity can be a significant problem if such monodispersed particles are to be used as an industrial product, despite their ideally controlled properties. In addition, taking into account the reaction conditions used to prepare AACH, such as relatively high temperature (≥50 °C)[1–3,9,20] and pressure,[2,9,21] long reaction time (≥24 h),[1–3,9] significant excess of $(NH_4)_2CO_3$ as a precipitant (molar ratio of $(NH_4)_2CO_3$ to Al^{3+} ≥4),[2,9,20,21] subsequent separation of the precipitate by filtration[1,3,14,20,21] or centrifugation,[3] and its washing, this procedure is costly for mass-produced products. Therefore, in contrast to published works, the present work focuses on reaction conditions that are interesting from a technological point of view for large-scale production.

The aim of this work is to design simpler and cheaper preparation route from a nearly saturated aqueous solution of $Al(NO_3)_3$ in the acid region, leading to formation of especially stable polynuclear $[Al_{13}O_4(OH)_{24}(H_2O)_{12}]^{7+}$ complex cations,[28] which are the dominant species found in solution at pH < 4.[10] This aluminium cluster (Al_{13}) with the Keggin structure, which consists of a central tetrahedral AlO_4 unit surrounded by 12 AlO_6 octahedra, is an important "green" solution precursor for large-area preparation of Al_2O_3 thin films and nanoparticles.[10,27]

This work focused on

- Preparation of aluminium clusters (Al_{13}) by partially neutralising a nearly saturated aqueous solution of $Al(NO_3)_3$ with $(NH_4)_2CO_3$ as a base at pH < 4 by the sol–gel method.
- Simplifying the process by eliminating washing and filtration, and energy saving by using a low processing temperature (22 °C).

• The effect of low solubility aluminium hydroxide acetate ($Al(OH)(CH_3COO)_2$) as a nucleating agent on the morphology, specific surface area, and pore size distribution (PSD) of the final alumina products prepared by thermal decomposition of synthesised alumina gels.

2. Experimental

2.1 Material synthesis

Aluminium nitrate nonahydrate ($Al(NO_3)_3 \cdot 9H_2O$, ACS reagent grade, ≥98%, Merck, KGaA, Darmstadt, Germany), ammonium carbonate ($(NH_4)_2CO_3$, ACS reagent grade, ≥30% NH_3 basis, Merck), aluminium hydroxide acetate hydrate ($Al(OH)(CH_3COO)_2 \cdot H_2O$, purity ≥28% Al_2O_3, Merck), and deionised water were used as the starting chemicals without further purification.

Synthesis of the alumina precursors was performed in a stirred reactor equipped with a mechanical stirrer. Typically, the exact amount (2–4 g) of $Al(OH)(CH_3COO)_2 \cdot H_2O$ powder was dispersed in 5 mL of 2.44 M $Al(NO_3)_3$ aqueous solution with pH = 0.2 and stirred with a constant agitation speed of 500 rpm until a homogeneous suspension formed. Subsequently, the calculated amount of 2.17 M $(NH_4)_2CO_3$ (pH = 8.5) was added drop-wise from a burette (1 mL min^{-1}) to the suspension with constant stirring and pH monitoring. The amount of added $(NH_4)_2CO_3$ solution was selected so that after mixing the resulting pH was ≤ 4. After 1 h stirring, the white colloid solution or gel was transferred into a teflon mould (3 cm × 3 cm) and dried at 22 °C under reduced humidity (Concept OV 1000 dehumidifier). The prepared alumina precursors were then calcined at different temperatures (220–1100 °C) for 2 h with a heating rate of 3.75 °C min^{-1}. The proposed procedure is schematically shown in Fig. 1.

2.2 Characterisation

The size of the particles was determined with a particle size analyser (Mastersizer 2000S, Malvern, UK) in deionised water by ultrasonic treatment. The thermal gravimetric analysis and differential thermal analysis (TG-DTA) measurements were

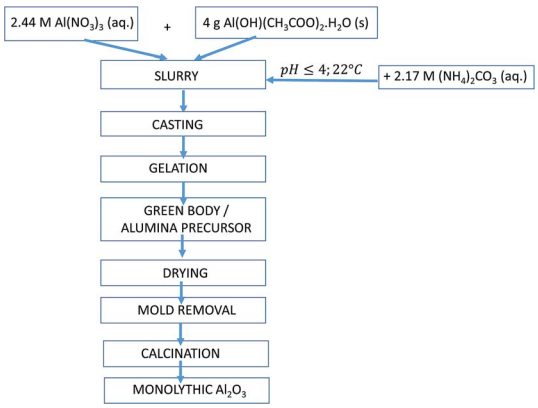

Fig. 1 Flow chart of the proposed process for production of nanoporous alumina monoliths.

Table 1 Experimental conditions used in the experiments and the properties of the prepared alumina precursors in each stage of preparation[a]

Sample	Selected $(NH_4)_2CO_3 : Al(NO_3)_3$ molar ratio	Initial suspension $Al(NO_3)_{3(aq)}$ + $Al(OH)(CH_3COO)_{2(s)}$ (AA)			+ Base $(NH_4)_2CO_{3(aq)}$	Final mixture/prepared alumina precursor			Alumina precursor consistency		
		$n_{Al(NO_3)_3}$ [mol]	m_{AA} [g]	$pH_{initial}$	$V_{(NH_4)_2CO_3}$ [dm^3]	pH_{final}	After 1 h stirring	After 72 h drying	Upon exposure to air
1	2.25 : 2	0.0122	2	0.67	0.0063	3.73	Liquid	Compact solid with a smooth glossy surface	"Cotton wool" surface
2	2.25 : 2	0.0122	4	0.95	0.0063	3.94	Liquid	Compact solid with a smooth glossy surface	Compact solid with a smooth glossy surface
3	2.75 : 2	0.0122	2	0.67	0.0078	4.09	Gel	Compact solid with a rough surface	Diffluent surface
4	2.75 : 2	0.0122	4	0.95	0.0078	4.18	Thick foam	Compact solid with a rough surface	Compact solid with a rough surface

[a] All of the experiments were performed at $T = 22$ °C and agitation speed of 500 rpm using $c_{Al(NO_3)_3} = 2.44$ mol dm^{-3}, $V_{Al(NO_3)_3} = 0.005$ dm^3, and $c_{(NH_4)_2CO_3} = 2.17$ mol dm^{-3}.

performed with a NETZCH STA 449F3 Jupiter analyser with a SiC furnace under a N_2 atmosphere at a heating rate of 10 °C min^{-1}. The powder X-ray diffraction (XRD) patterns were obtained with an X-ray powder diffractometer (Rigaku Mini-Flex 600) with Cu-K_α radiation (with a Ni filter) operated at 40 kV and 15 mA. Diffraction was performed from $2\theta = 5°$ to 90° at a rate of 2° min^{-1}. The nature of the bonding in the samples was determined by infrared (IR) spectroscopy and ^{27}Al NMR spectroscopy. Fourier transform IR (FT-IR) spectroscopy at a resolution of 4 cm^{-1} was performed with a Nicolet 6700 FT-IR spectrometer (Thermo Scientific) using a Smart orbit device. The ^{27}Al NMR spectra were recorded with a solid-state NMR spectrometer (Varian 400 MHz, Palo Alto, CA, USA) at a Larmor frequency of 104.18 MHz using a probe head with a 4 mm rotor at a magic angle spinning rate of 12 kHz. 3100 scans were accumulated with a recycle delay of 5 s with the rf pulse length of 0.235 s corresponding to the flip angle of 9° for the central transition in solids. The spectra were processed with Varian Vnmrj 3.2 and Mestrelab Mnova 12.0 software. A 1 mol dm^{-3} aqueous $[Al(H_2O)_6]^{3+}$ solution (primary standard) was used as the reference for the chemical shifts. The textural properties of the prepared samples were measured through the nitrogen adsorption/desorption isotherms (NOVA 1000e, Quantachrome Instruments, USA). Prior to the measurements, the samples were outgassed at different temperatures (110–290 °C) for 20 h. The specific surface area was determined by the multipoint ($S_{A,M}$) Brunauer–Emmett–Teller (BET) method using the adsorption data in the relative pressure range $0.05 \leq p/p_0 \leq 0.35$, and the *t*-plot and α_S-plot methods were used to evaluate the microporosity. The PSDs were derived from the adsorption/desorption branches of the isotherms using the Barrett–Joyner–Halenda (BJH) model. The pore volume (V_p) was calculated from the adsorbed volume of gas at different relative pressures (p/p_0), and the results were evaluated on the basis of density functional theory (DFT). The pore size distribution was calculated by NLDFT adsorption model (non-local DFT) under conditions of adsorbate of N_2 77 K and adsorbent of zeolite/silica for the cylindrical-spherical pores. Scanning Electron Microscopy (SEM) observations were performed on a TESCAN Mira 3 using 30 kV accelerating voltage at a working distance of 8.94 mm.

3. Results and discussion

3.1 Effect of the reaction conditions on alumina precursor formation

Polynuclear $[Al_{13}O_4(OH)_{24}(H_2O)_{12}]^{7+}$ complex cations (known as Keggin ε-Al_{13} ions) were synthesised by partial neutralisation of Al^{3+} solution with a base at OH^-/Al^{3+} molar ratios from 0.5 to 2.5, corresponding to pH values less than 4.[10,24,27] The results of mechanochemical synthesis of polymeric ε-Al_{13} ions in the concentrated state between $[Al(H_2O)_6]Cl_3$ and $(NH_4)_2CO_3$ have shown that the maximum concentration of ε-Al_{13} species (85%) is achieved at a molar ratio of $CO_3^{2-} : Al^{3+} = 2.55 : 2$.[24] In this study, two different molar ratios of $(NH_4)_2CO_3$ to $Al(NO_3)_3$ within the surrounding range ($n_{CO_3}{}^{2-} : n_{Al}{}^{3+} = 2.25 : 2$ and 2.75 : 2) were used to prepare Al_{13} clusters as a solution precursor of Al_2O_3. To control the textural properties of the final Al_2O_3 product, various amounts of low solubility aluminium hydroxide acetate hydrate ($Al(OH)(CH_3COO)_2 \cdot H_2O$) were added to the $Al(NO_3)_3$ solution before base addition. It was hypothesised that chelation of aluminium ions with acetate ions could affect the stability of precursor colloid solution,[8] the structure of the formed aluminium hydroxide gel, and thus the textural characteristics of the final Al_2O_3. In addition, $Al(OH)(CH_3COO)_2OH \cdot H_2O$ particles as crystallisation centres could contribute to lowering the transformation temperature of the prepared aluminium gel to various forms of Al_2O_3.

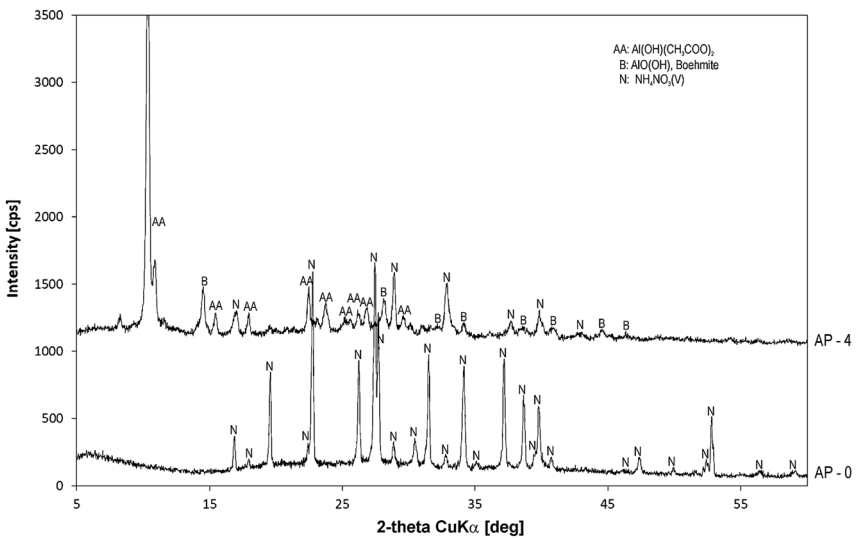

Fig. 2 XRD patterns of the prepared alumina precursor with 4 g $Al(OH)(CH_3COO)_2$ (AP-4) and without addition of $Al(OH)(CH_3COO)_2$ (AP-0). Abbreviations: AA: $Al(OH)(CH_3COO)_2$ (ICDD 00-004-0113); B: boehmite AlO(OH) (ICDD 01-083-1506); N: NH_4NO_3 (AP-0, ICDD 00-008-0499 and ICCD 01-083-0520; AP-4, ICDD 01-083-0520).

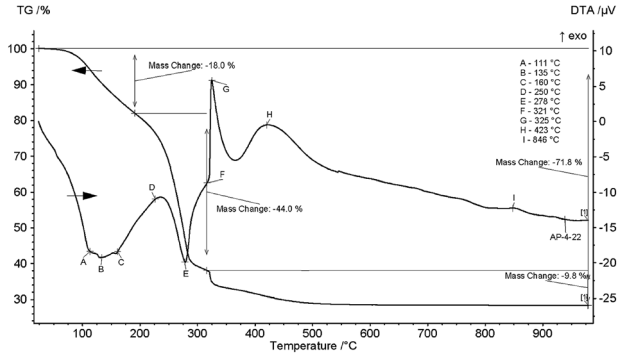

Fig. 3 TG–DTA curves of the prepared alumina precursor with 4 g $Al(OH)(CH_3COO)_2$ (AP-4).

Particle size analysis of the $Al(OH)(CH_3COO)_2 \cdot H_2O$ powder showed that 90% of the particles had mean size $d(90) \leq 18.8$ μm. The experimental conditions are given in Table 1.

Taking into account the properties of the prepared samples during synthesis and after drying (Table 1), in relation to handling under technological conditions, only sample 2 was considered to be a suitable alumina precursor for further study. The reason for its selection was the longer gelation time (up to 48 h) than the other samples. This provides longer time for handling the precursor, as well as its stable compact form, which does not undergo surface dehydration when exposed to air. Rapid dehydration of the surface of the Keggin-type aluminium clusters is attributed to the loss of less tightly bound water molecules that contract the crystals and disrupt the crystal surface,[29] as confirmed by formation of "cotton wool" on the surface of sample 3 within 1 week.

The XRD pattern of the selected alumina precursor (sample 2 in Table 1) obtained at a molar ratio of CO_3^{2-} to $Al^{3+} = 2.25 : 2$ with 4 g of aluminium hydroxide acetate as a nucleation additive is shown in Fig. 2. For easier identification of the formed (oxy) hydroxide phases, the peaks of aluminium hydroxide acetate (AA) and ammonium nitrate (N) formed as a by-product of the reaction are also assigned in the XRD pattern. The effect of aluminium hydroxide acetate on the type of aluminium hydroxide oxide can be seen by comparison with the diffractogram of the sample prepared under the same reaction conditions but without addition of aluminium hydroxide acetate (AP-0).

The results of XRD analysis revealed that the selected alumina precursor was composed of a mixture of crystalline NH_4NO_3 (ICDD 01-083-0520), $Al(OH)(CH_3COO)_2$ (ICDD 00-004-0113), and boehmite (ICDD 01-083-1506). The broad diffraction peaks of the boehmite phase (γ-AlO(OH)) indicated that it had low crystallinity, which is related to the high concentration of Al^{3+} and hence to the high nucleation rate, resulting in formation of small particles.[20] From Fig. 2, for the sample without addition of $Al(OH)(CH_3COO)_2$, the boehmite phase (despite its higher proportion in the mixture) did not form, suggesting that aluminium hydroxide acetate had a significant effect on boehmite formation.

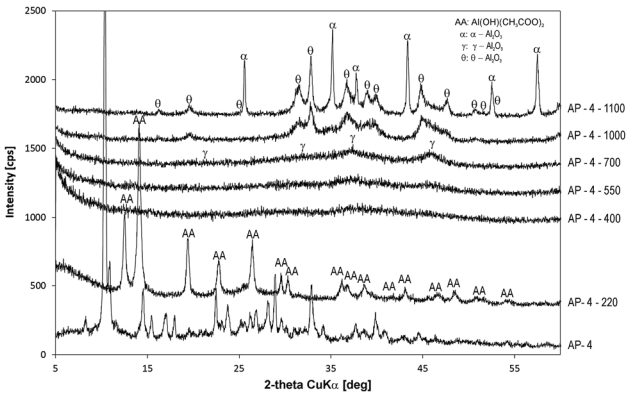

Fig. 4 XRD patterns of the prepared alumina precursor (AP-4) and its thermal decomposition products after calcination at different temperatures for 2 h. Abbreviations: AA: $Al(OH)(CH_3COO)_2$ (ICDD 00-013-0833); α: α-Al_2O_3 (ICDD 01-089-3072); γ: γ-Al_2O_3 (ICDD 00-010-0425), θ: θ-Al_2O_3 (ICDD 01-035-0121).

Table 2 Theoretical mass loss of the prepared alumina precursor derived by mass balance calculations

					Prepared alumina precursor		
	Reactants		Additive		Products		Additive
Stoichiometric molar ratio	**$Al(NO_3)_3$** 2 mol	**$(NH_4)_2CO_3$** 3 mol	$Al(OH)(CH_3COO)_2$	→	**AlO(OH)** 2 mol	**NH_4NO_3** 6 mol	$Al(OH)(CH_3COO)_2$
Used molar ratio	**2 mol**	**2.25 mol**	—	→	**2 mol**	**5 mol**	—
Input amount n_i [mol]	0.0122	0.0137	0.022	Output amount n_i [mol]	0.0122	0.0274	0.022
Input mass $m_i = n_i M_i$ [g]	2.599	1.315	4	Output mass $m_i = n_i M_i$ [g]	0.732	2.192	4
				Mass before calcination [g]	6.924		
				Theoretical mass loss of individual component w_i [%]	15	100	71.67
				Mass after calcination [g]	0.622 1.755	0	1.133
				Theoretical mass loss of the alumina precursor w_i [%]	**74.7**		

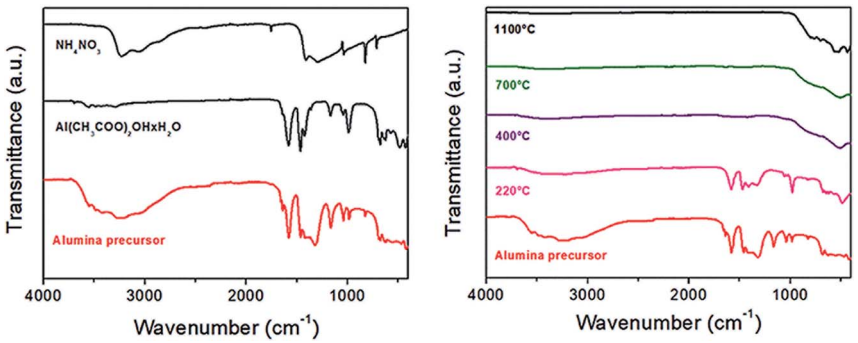

Fig. 5 FT-IR spectra of the prepared alumina precursor compared with the spectra of its individual components (left side) and calcined products prepared at different temperatures (right side).

3.2 Thermal transformation of the prepared alumina precursor to Al_2O_3

Upon heating, boehmite sequentially transforms to γ-alumina, δ-alumina, θ-alumina, and α-alumina.[30] Determination of the suitable calcination temperature for preparation of active alumina with a nanoporous structure was performed by TG–DTA. The TG–DTA curves obtained from decomposition of the prepared alumina precursor are shown in Fig. 3.

The thermogravimetric curve showed that weight loss occurred in several steps, corresponding to the reactions associated with NH_4NO_3 decomposition and transformation of $Al(OH)(CH_3COO)_2 \cdot H_2O$ and γ-AlO(OH) to Al_2O_3.

The gradual weight loss up to 200 °C is related to release of part of the –OH and acetate groups (18%), while the sharp weight loss above 200 °C (44%) is correlated with simultaneous removal of residual acetate groups and decomposition of NH_4NO_3.[31,32] The significant exothermic peak centred around 325 °C corresponds to combustion of released acetate groups (as "fuel") with NH_4NO_3 as an oxidising agent. The broad exothermic peak at 423 °C is ascribed to transformation of boehmite to γ-Al_2O_3,[20] and the slight exothermic peak at around 846 °C is attributed to gradual formation of the θ-Al_2O_3 crystalline structure, which is in good agreement with XRD analysis of boehmite annealed at temperatures up to 1000 °C.[30] The total weight loss at 1000 °C was 71.8%, which is in agreement with the theoretical value of 74.7% (Table 2), and the individual stages of decomposition are in accordance with the published TG–DTA data of the individual components.[20,31,32]

The prepared alumina precursor was calcined at 220–1100 °C, and the nitrogen adsorption–desorption isotherms were immediately measured after calcination to evaluate the textural properties. Calcination at 220 °C was performed to remove the NH_4NO_3 by-product from the precursor. Transformation of the boehmite (γ-AlO(OH)) formed in the mixture with $Al(OH)(CH_3COO)_2$ into various forms of Al_2O_3 was observed at temperatures above 220 °C.

By heat treatment, aluminium (oxy)hydroxides pass through a series of phase transitions during which the hydroxyl groups are removed. Because of the different degrees of dehydroxylation, these intermediates (so-called transition aluminas) exhibit structural differences resulting from the variability of

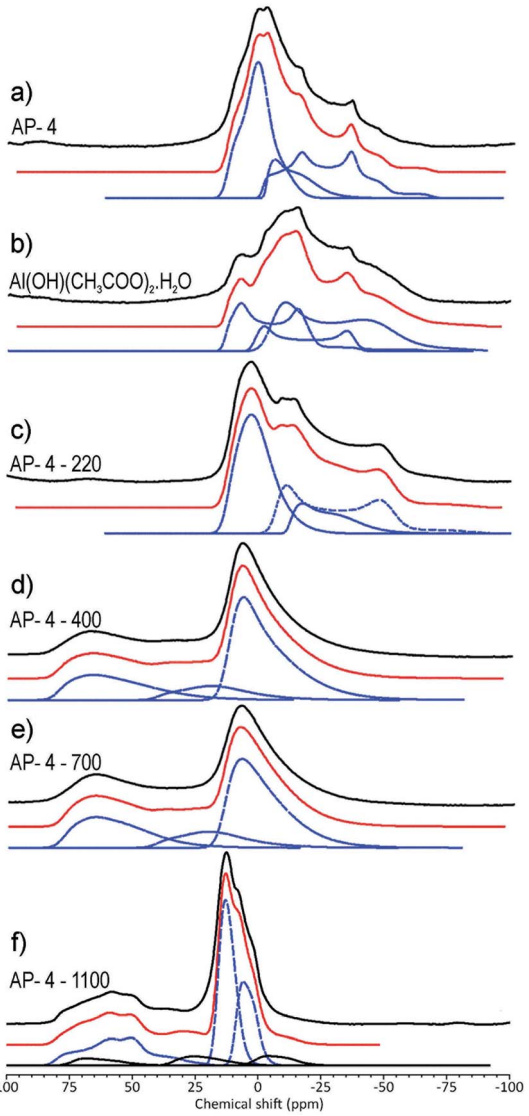

Fig. 6 ^{27}Al NMR spectra of the (a) prepared Al_2O_3 precursor (AP-4), (b) $Al(OH)(CH_3COO)_2 \cdot H_2O$, and the prepared Al_2O_3 precursor calcined at (c) 220, (d) 400, (e) 700, and (f) 1100 °C (black: experimental; color: simulated).

Table 3 ^{27}Al solid-state NMR parameters of the studied samples (isotropic chemical shift δ_{iso}, quadrupole coupling constant C_Q, asymmetry parameter η_Q, line broadening Δ, and occupancy of the Al site)

Sample	Aluminium site	δ_{iso} [ppm]	C_Q [MHz]	η_Q	Δ [Hz]	Occupancy [%]
Prepared alumina precursor	Al_6 (1)	13.2	4.1 ± 0.7	1.0 ± 0.1	500	48.1
	Al_6 (2)	2.9	7.1 ± 0.2	0.4 ± 0.1	250	37.2
	Al_6 (3)	0.65	4.9 ± 1.6	0.2 ± 0.05	100	14.7
Aluminium hydroxide acetate hydrate	Al_6 (1)	11.0	7.5 ± 0.1	0.1 ± 0.05	400	17.7
	Al_6 (2)	19.0	6.6 ± 0.2	0.2 ± 0.15	300	33.1
	Al_6 (3)	5.5	8.1 ± 1.3	0.1 ± 0.05	800	49.2
Boehmite 220 °C	Al_6 (1)	13.35	4.5 ± 1.6	0.65 ± 0.1	600	50.5
	Al_6 (2)	3.8	8.1 ± 0.6	0.1 ± 0.1	450	34.9
	Al_6 (3)	−8.7	5.8 ± 1.8	0.2 ± 0.05	250	14.6
γ-Al_2O_3 400 °C	Al_4	83.0	6.8 ± 2.6	0.4 ± 0.1	700	24.4
	Al_5	41.0	6.2 ± 2.0	0.4 ± 0.1	800	12.6
	Al_6	15.3	5.6 ± 3.3	0.4 ± 0.1	700	63.0
γ-Al_2O_3 700 °C	Al_4	81.0	6.4 ± 2.1	0.4 ± 0.1	700	27.3
	Al_5	42.0	6.2 ± 2.0	0.7 ± 0.1	800	14.6
	Al_6	16.9	5.5 ± 2.8	0.3 ± 0.1	700	58.1
α- and θ-Al_2O_3 1100 °C	Al_4	81.2	6.5 ± 2.0	0.65 ± 0.1	600	25.0 (θ)
	Al_6 (1)	16.6	2.9 ± 0.9	0.0	500	38.8 (α)
	Al_6 (2)	9.7	3.2 ± 0.6	0.0	450	20.7 (θ)
	Al_4	78.0	5.1 ± 1.5	0.25 ± 0.1	800	4.2
	Al_5	42.0	6.0 ± 1.5	0.4 ± 0.1	500	6.5
	Al_6	4.0	4.5 ± 0.8	0.3	700	4.8

the aluminium coordination numbers, which is reflected in poorly resolved X-ray diffractograms.[30] This phenomenon is also evident from the diffractograms (Fig. 4) of the prepared alumina precursor (AP-4, Fig. 2) calcined in the temperature range 400–700 °C, which show formation of gel-type X-ray amorphous phases, which were identified by ^{27}Al NMR. In the range 700–1000 °C, γ-Al_2O_3 (ICDD 00-010-0425) transformed to θ-Al_2O_3 (ICDD 01-035-0121), and above 1100 °C θ-Al_2O_3 recrystallised to α-Al_2O_3 (corundum, ICDD 01-089-3072).

The nature of bonding in the prepared alumina precursor and its calcined products obtained at different calcination temperatures was characterised by FT-IR analysis (Fig. 5). The IR spectra of the precursor and its individual accompanying admixtures, such as aluminium acetate hydroxide and ammonium nitrate, are shown in the left part of Fig. 5. The IR spectrum of the prepared sample confirmed the presence of all of the functional groups from NH_4NO_3 (ν(N–H) = 3228, 3061 cm^{-1}; $\delta(NO_3)$ = 1409, 1295 cm^{-1}) and $Al(OH)(CH_3COO)_2 \cdot H_2O$ (ν(O–H) = 3554, 3487, 3292 cm^{-1}; ν(C=O) = 1582 cm^{-1}; $\delta(CH_3)$ = 1464, 1423 cm^{-1}; ν(C–C) = 1041, 987 cm^{-1}; ν(Al–O) = 675, 625, 482, 428 cm^{-1}).

The IR spectra of the prepared precursor and its calcined products are compared in the right side of Fig. 5. The IR spectrum of the sample calcined at 220 °C only contained absorption bands originating from aluminium hydroxide acetate (ν(C=O) = 1581 cm^{-1}; $\delta(CH_3)$ = 1471, 1408, 1331 cm^{-1}; ν(C–C) = 980 cm^{-1}; ν(Al–O) = 486 cm^{-1}), while the bands assigned to ammonium nitrate disappeared, indicating its complete decomposition, which is consistent with the results of TG–DTA analysis (Fig. 3). The IR spectra of the samples calcined at higher temperatures (400, 700, and 1100 °C) only contained the ν(Al–O) absorption band, confirming the presence of aluminium oxide. Moreover, the different numbers and positions of the ν(Al–O) absorption bands indicated different modifications of the final products due to phase transformation from γ-Al_2O_3 through θ−Al_2O_3 to α−Al_2O_3, which are related to the different coordination of Al^{3+} (hexa-coordinated AlO_6, penta-coordinated AlO_5 and tetra-coordinated AlO_4),[8,9,33–36] and is in accordance with the results of X-ray analysis (Fig. 4). The samples calcined at 400 and 700 °C both showed one band at 509 cm^{-1}. The sample calcined at 1100 °C showed absorption bands at 702, 633, 559, 521, and 436 cm^{-1}.

Because transformation between the distinct intermediate phases is a gradual process, the exact temperatures to obtain the individual phases cannot be determined solely by XRD experiments.[13] A reliable tool that allows unambiguous identification of these phases is ^{27}Al solid-state NMR.[13,30] Clarification

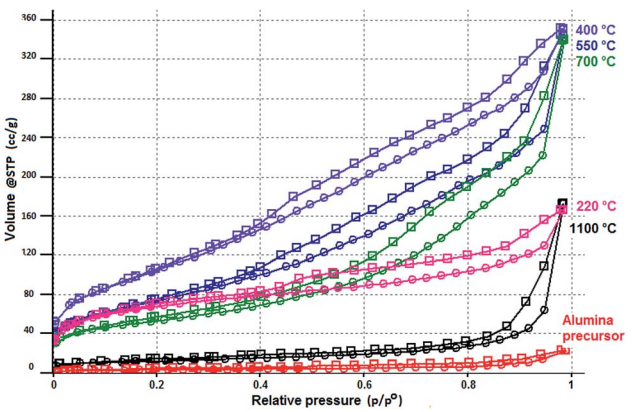

Fig. 7 N_2 adsorption–desorption isotherms of the prepared alumina precursor and its calcined products obtained at different temperatures.

Table 4 Comparison of the textural parameters of the prepared alumina precursor and its calcined products obtained at different temperatures

Sample	Specific surface area $S_{A,M}$ $P_{rel} \in (0.05–0.35)$ [$m^2\ g^{-1}$]	Evaluation of the porosity by the *t*-plot method [$m^2\ g^{-1}$]		Micropore volume evaluated by the α_s-plot method [$cm^3\ g^{-1}$]	V_{tot} determined from desorption [$cm^3\ g^{-1}$]			Average pore diameter [nm]
		$S_{A,micro}$	$S_{A,ext}$ [a]		$d < 2$ nm	$d < 20$ nm	$d < 135$ nm	$P_{rel} \in (0–0.99)$
Alumina precursor	9	0	9	0	0.006	0.02	0.035	15
220 °C	224	107	114	0.072	0.108	0.19	0.26	4.5
400 °C	376	55	320	0.102	0.162	0.48	0.63	5.6
550 °C	267	0	267	0.041	0.116	0.38	0.53	8
700 °C	184	0	185	0.005	0.088	0.35	0.52	11
1100 °C	41	0	41	0	0.020	0.08	0.26	26

[a] $S_{A,ext}$ - meso-, macropores and external surface.

of the structures of the prepared Al_2O_3 precursor and its heat-treated products was performed by ^{27}Al NMR measurements.

The ^{27}Al NMR spectra of transition aluminas show signals characteristic of tetra-coordinated AlO_4, hexa-coordinated AlO_6 and penta-coordinated AlO_5.[30] Simulations of the spectra provide the NMR parameters: the isotropic chemical shift δ_{iso}, quadrupole coupling constant C_Q, and asymmetry parameter η_Q. The Al coordination is reflected in isotropic chemical shift values.[13,30] The quadrupole coupling constant C_Q (in MHz) reflects distortion from a perfect octahedron or tetrahedron, *i.e.*, a large C_Q value means distorted Al sites. Simulation of the ^{27}Al NMR spectra (Fig. 6a–f) using the QuadFit program[37] are given in Table 3.

The spectrum of the prepared Al_2O_3 precursor (Fig. 6a) showed features between 25 and −75 ppm. The isotropic chemical shift values were in the range typical of hexa-coordinated aluminium (AlO_6). The first line with a δ_{iso} value of 13.2 ppm can be assigned to boehmite, although its C_Q value was larger than that reported by Chandran *et al.*[30] This can be explained by the larger disorder in the prepared precursor owing to the presence of aluminium acetate, which probably gives rise to the other two lines in the spectrum with relatively large C_Q values. The ^{27}Al NMR spectrum of pure aluminium acetate (Fig. 6b) consisting of signals in the range typical of hexa-coordinated aluminium was tentatively simulated using three lines with relatively large C_Q and low η_Q values (Table 3). The difference between the NMR parameters obtained for aluminium acetate in the prepared Al_2O_3 precursor and those of the pure chemical can be attributed to the obvious difference between the ^{27}Al environments in the pure compound and prepared material. Calcination of the prepared alumina precursor at 220 °C (Fig. 6c) resulted in a slightly different shape of the NMR spectrum, in which there was still evidence for the presence of aluminium acetate. Calcination at 400 °C (Fig. 6d) was expected to completely remove aluminium acetate from the sample and induce a phase transition to γ-alumina.

γ-Alumina crystallises in the spinel structure, where Al^{3+} ions occupy tetrahedral and octahedral interstitial sites,[12] with some degree of crystallographic distortion related to the presence of penta-coordinated Al(v) species.[13,30,38,39] The simulations of the spectra measured after calcination at 400 and 700 °C (Fig. 6d and e) confirmed signals with isotropic chemical shift values characteristic of tetra-, hexa- and penta-coordinated aluminium.[30] However, the respective C_Q values were larger than the reported values, which indicates a large deviation from spherical symmetry, probably caused by the presence of aluminium acetate in the course of sample preparation. Calcination at 1100 °C (Fig. 6f) resulted in phase transitions to θ- and α-alumina. The C_Q and η values (Table 3) were in agreement with those reported in the literature.[30]

The textural properties of the prepared alumina precursor and its calcined products obtained at different temperatures were determined by N_2 adsorption–desorption measurements (Fig. 7), and the results are summarised in Table 4.

The shapes and relative positions of the curves in Fig. 7, as well as the results in Table 4, indicate the changes that occurred during thermal treatment of the prepared precursor.

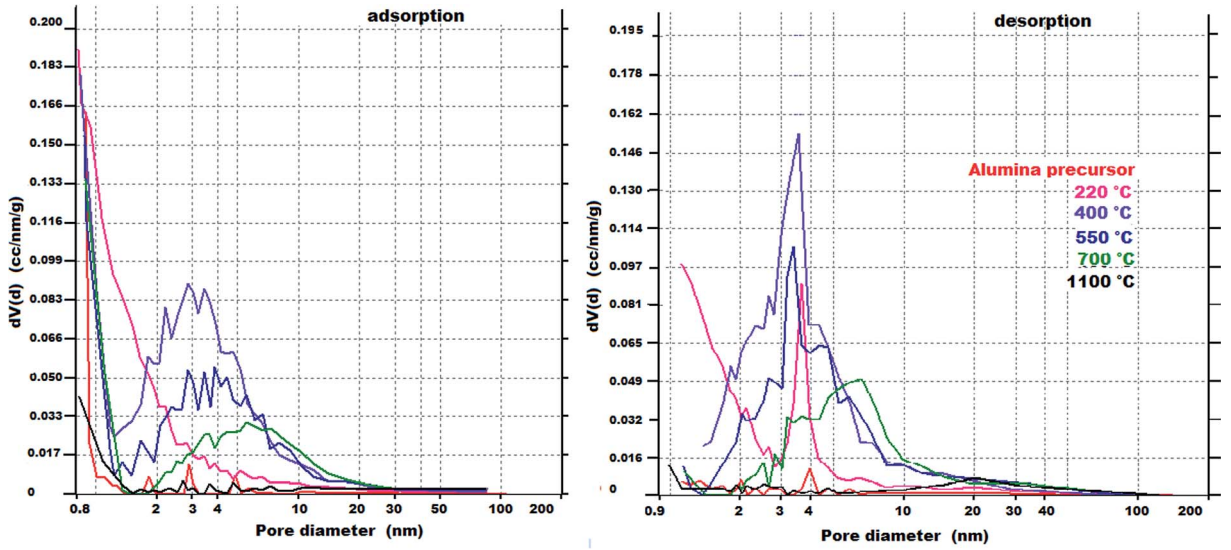

Fig. 8 PSDs of the prepared alumina precursor and its calcined products obtained at different temperatures determined by BET analysis using the BJH model.

From the values in Table 4, the prepared alumina precursor had a very low specific surface area ($S_A = 9\ m^2\ g^{-1}$). However, its subsequent calcination at 220 °C (associated with removal of NH_4NO_3) led to development of micro- (<2 nm) and mesopores (2–50 nm), which was accompanied by a significant increase in the surface area (224 $m^2\ g^{-1}$). The presence of mesopores is indicated by a characteristic hysteresis loop that closes at a relative pressure of ~0.4. Heating to 400 °C caused a further increase in the specific surface area (376 $m^2\ g^{-1}$), while the proportion of micropores decreased. The considerable increase in S_A up to 400 °C can be attributed to gaps left by the gas molecules released by both decomposition of NH_4NO_3 and $Al(OH)(CH_3COO)_2$ and dehydroxylation of boehmite (AlO(OH)) to γ-Al_2O_3 (see Fig. 3). Calcination above 550 °C was associated with a gradual decrease of the specific surface area because of recrystallisation and sintering of alumina nanoparticles.

The PSDs of the prepared alumina precursor and its calcined products obtained at different temperatures determined from the adsorption/desorption curves (dV/d) by the BJH method are shown in Fig. 8, and the volume histograms determined by DFT[40] are shown in Fig. 9.

From Fig. 8 and 9, although the precursor before calcination had a low specific surface area (9 $m^2\ g^{-1}$), it contained micropores with sizes less than 1 nm. Calcination at 220 °C led to development of micropores. For calcination at 400 °C, mesopores with a narrow bimodal distribution (maxima at 3 and 10 nm) accounted for the significant increase in the pore volume.

At temperatures above 400 °C, the micropores disappeared and the mesopores became larger, leading to a decrease in the

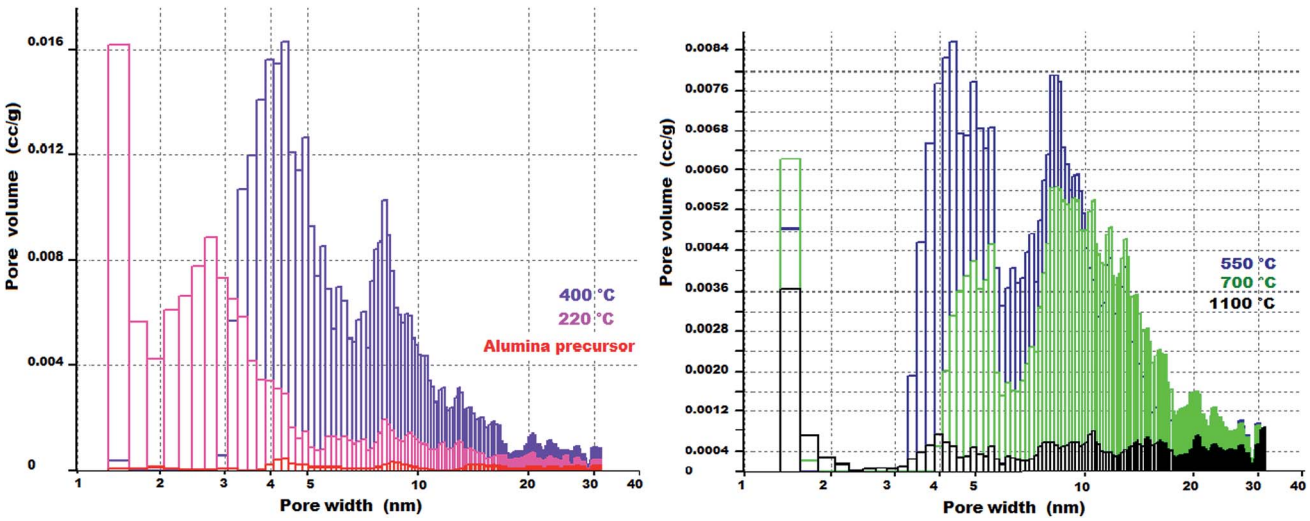

Fig. 9 Pore volume histograms of the prepared alumina precursor and its calcined products obtained at different temperatures determined by DFT.

Table 5 Comparison of the textural parameters of the prepared Al_2O_3 and products synthesised by thermal decomposition of ammonium aluminium carbonate hydroxide (AACH) at comparable calcination temperatures

Method of preparation of alumina precursor	Alumina source	Base	pH	Semiproduct	Calcination temperature and time	Pore characteristics of Al_2O_3			Lit.
						Surface area (BET) [$m^2\ g^{-1}$]	Total pore volume [$cm^3\ g^{-1}$]	Average pore diameter [nm]	
Precipitation	0.11 M $Na[Al(OH)_4]_{(aq)}$	$(NH_4)_2CO_3$ (aq)	10	$NH_4Al(OH)_2CO_3$	400 °C/3 h	618.68[a]	0.54[a]	4.43[a]	3
					500 °C/3 h	552.77[a]	0.55[a]	4.71[a]	
	0.13 M $Al(NO_3)_3 \cdot 9H_2O_{(et)}$	$(NH_4)_2CO_3$ (aq)	7.5	$AlO(OH) \cdot nH_2O$	600 °C/5 h	260.8	1.80	20.6	1
			8.5	$AlO(OH) \cdot nH_2O$ + $NH_4AlO(OH)HCO_3$		276.6	2.08	6.9; 39.7	
			9.5	$NH_4AlO(OH)HCO_3$		290	2.41	7.3; 49.5	
	1.2 M $Al(NO_3)_3 \cdot 9H_2O_{(aq)}$	$(NH_4)_2CO_3$ (aq)	7–8	$NH_4Al(OH)_2CO_3$	500 °C/4 h	407	1.17	2.7–29.3	20
	0.4 M $AlCl_3 \cdot 6H_2O_{(aq)}$	NH_4HCO_3 (aq)	>7	$NH_4Al(OH)_2CO_3$	600 °C/5 h	325	0.73	5.5	21
Hydrothermal synthesis	$Al(OH)_3$ xerogel (70 wt% Al_2O_3)	NH_4HCO_3 (aq)	10.5	$NH_4Al(OH)_2CO_3$	350 °C/2 h	441	0.67	6.8	9
					500 °C/2 h	246	0.7	10.7	
	0.4 M $AlCl_3 \cdot 6H_2O_{(aq)}$	$(NH_4)_2CO_3$ (aq)	>7	$NH_4Al(OH)_2CO_3$	600 °C/2 h	300	0.44	4.2	21
Solid-state	$AlCl_3 \cdot 6H_2O_{(s)}$	$(NH_4)_2CO_3$ (s)		$NH_4Al(OH)_2CO_3$	600 °C/2 h	298	0.99	9.7	21
Sol–gel	2.44 M $Al(NO_3)_3 \cdot 9H_2O_{(aq)}$ + $Al(OH)(CH_3COO)_{2(s)}$	$(NH_4)_2CO_3$ (aq)	3.8	$AlO(OH)$	400 °C/2 h	376	0.63	5.6	This
					550 °C/2 h	267	0.53	8.0	work

[a] Values obtained at slow heating rate (5 °C min^{-1}).

pore volume, which is related to agglomeration of Al_2O_3 crystallites. The complete disappearance of the microporosity at higher temperature (>400 °C) is probably associated with loss of the intracrystalline porosity owing to sintering, which is a typical phenomenon, especially when sintering small particles.[20] Nevertheless, it is important to emphasise that the γ-Al_2O_3 synthesised in this work shows comparable parameters of open porosity than those synthesised by thermal decomposition of ammonium aluminium carbonate hydroxide (AACH) at comparable calcination temperatures – Table 5.

It can be assumed that the textural characteristics of the nanoporous Al_2O_3 (Table 4) are probably influenced by the addition of $Al(OH)(CH_3COO)_2$ which as a component of the prepared alumina precursor acts as a textural modifier. This assumption is based on the fact, that the acetate anions (OAc^-) formed by partial dissociation of $Al(OH)(CH_3COO)_2$ (ref. 41) initially combine with Al^{3+} cations in $[Al_{13}O_4(OH)_{24}(H_2O)_{12}]^{7+}$ complex cluster into a binuclear mixed-hydroxo species $[Al_2(OH)_2OAc)]^{3+}$, in which acetate ion acting as a bridge between the apices of two dihydroxo-bridged Al(III) octahedra.[42–44] Chelation of aluminium ions with acetate ions could, like the citric acid[11] or phosphoric acid,[45] affect the stability of the colloidal solution[8] and thus also the structure of the aluminium hydroxide gel formed around the undissociated part of $Al(OH)(CH_3COO)_2$ and/or the structure of the final Al_2O_3 product. With increasing pH, the concentration of $[Al_2(OH)_2OAc)]^{3+}$ complex cluster cations increases, and at pH = 4 (*i.e.* at reaction conditions used in this work) strong predominance of the Al(III)- acetate complexes was confirmed.[42] The addition of OH^- will reduced the surface positive charge of polymeric Al-micelle thereby the hydroxyl bridges in polymeric Al are converted into oxygen bridges.[46]

The acetate ions are weakly chelating agent, so chelates formed between aluminium and acetate ions have a low stability constant. Since chelates of the lower stability constants provide higher supersaturation in the nucleation stage as well, they usually provide smaller particles with a narrow size distribution.[7,47]

This assumption is confirmed by the SEM image (Fig. 10) of the alumina monolith prepared by calcination at 400 °C for 2 hours at 100k× magnification.

The Fig. 10 shows a fiber-like structure morphology composed from thin nanofibers of about 100 nm in length with the diameter of about 5 nm leading to the formation of a highly porous material. The fibrous structure may be related to the –OH groups in the (010) and (100) facets of γ-AlO(OH) precursor, which could act as the adsorption site for anions.[47,48] The adsorption would decrease the surface energy and limit the aggregation of the γ-AlO(OH) nanoparticles on these facets, which would result in the oriented aggregation of γ-AlO(OH) along the (001) direction.[48] The adsorption ability of the acid anions is related to the charge/size ratio, and the anions with the larger charge/size ratio would be adsorbed more easily on the particle surface of γ-AlO(OH). Since acetate ions have a relatively high charge-to-size ratio (6.289) their strong adsorption on the particle surfaces of γ-AlO(OH) leads to the formation of nanorods that grew along the (001) direction.[48]

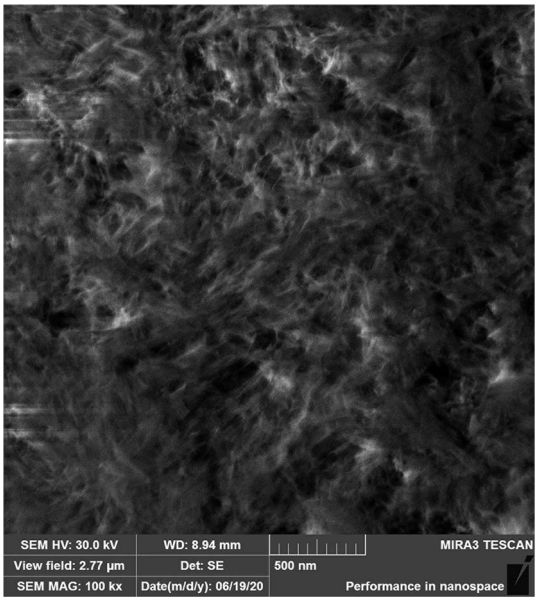

Fig. 10 SEM micrograph of prepared nanoporous alumina monolith calcined at 400 °C.

From the Fig. 10 it can be seen that the corresponding shape retained γ-Al_2O_3 was obtained after calcination.

It is important to emphasize the fact that the nanoporous alumina monolith was prepared without the use of surfactants, while according to the literature the monolithic alumina aerogels with hierarchically porous structure were prepared by sol–gel[5] or emulsion-gel casting[49] using aluminum isopropoxide with organic surfactant (Pluronic P 123[5], Sodium Dodecyl Sulfate (SDS)[49]). High price of aluminium alkoxides as alumina sources and surfactants cause that these are less attractive for large-scale production.[1] Thus, ammonium carbonate and aluminium nitrate which were used in this work are the reagents that are inexpensive, easily available and widely used in the chemical industry.[1]

In addition, the conclusions of previously published works on the preparation of $NH_4Al(OH)_2CO_3$ (AACH) as a precursor of nanostructured Al_2O_3 showed that boehmite (AlO(OH)) is an intermediate in the synthesis of AACH[1] and its excessive washing (due to its reactive nature in deionized H_2O)[20] as well as in its transformation to Al_2O_3.[3] In the context of these findings, the formation of boehmite prepared under the reaction conditions in this work (pH < 4; 22 °C) is an advantage in comparison to the preparation of AACH at pH > 7 and $T \geq 50$ °C in terms of prevention of particle aggregation, which is confirmed by the following published statements:

(a) Surface property of boehmite may mitigate the hard aggregation of particles during calcination because the interface hydrophobicity, determining by the contact angles (θ) of AACH, AlO(OH) and Al_2O_3 using water, increased in the order of AACH ($\theta = 30.82°$) > boehmite ($\theta = 33.79°$) > Al_2O_3/200 °C ($\theta = 53.45°$).[3]

(b) High temperature and pH values close to the boehmite point of zero charge PZC (pH = 8.2) favours strong aggregation.[20]

4. Conclusions

We have reported a simplified procedure for preparation of nanostructured compact alumina under technologically advantageous conditions.

(1) Alumina precursors for synthesis of nanoporous Al_2O_3 by thermal treatment were prepared by partial neutralisation of a nearly saturated aqueous solution of $Al(NO_3)_3$ with $(NH_4)_2CO_3$ as a base at pH < 4. Synthesis in the acidic region led to formation of polynuclear aluminium clusters (Al_{13}), which are important "green" solution precursors for preparation of active Al_2O_3 thin films and nanoparticles.

(2) Control of the textural properties of the final alumina during calcination of the prepared aluminium (oxy)hydroxide gels was accomplished by adding low solubility aluminium hydroxide acetate hydrate ($Al(OH)(CH_3COO)_2 \cdot H_2O$) as a nucleating agent to the $Al(NO_3)_3$ solution before neutralisation. It was found that $Al(OH)(CH_3COO)_2 \cdot H_2O$ affects the structure of the aluminium hydrated form formed around the nucleation centres and thus the structure of the forming intermediate aluminium oxide forms. It was confirmed that while addition of $Al(OH)(CH_3COO)_2 \cdot H_2O$ resulted in formation of the boehmite phase (γ-AlO(OH)), boehmite did not formed without the nucleating agent. This suggests that addition of aluminium hydroxide acetate as a nucleating agent has a significant effect on formation of boehmite.

(3) Considering the gelation time required for handling the precursor, as well as its stable compact form that is not surface dehydrated upon exposure to air, the molar ratio of $(NH_4)_2CO_3$ to $Al(NO_3)_3 = 2.25 : 2$ with addition of 4 g of $Al(OH)(CH_3COO)_2 \cdot H_2O$ (per 0.0122 moles of $Al(NO_3)_{3(aq)}$) were optimal.

(4) The large BET specific surface area (376 $m^2\ g^{-1}$) and relatively narrow pore distribution (2–20 nm) of the compact Al_2O_3 synthesised at 400 °C are likely to be because of the chelating effect of the acetate ions and the gases produced by decomposition of $Al(OH)(CH_3COO)_2 \cdot H_2O$ and the NH_4NO_3 by-product during calcination, which prevent agglomeration of Al_2O_3 particles. The heat released by decomposition of NH_4NO_3 can also contribute to preserving the textural properties during transformation of boehmite to transition aluminas by lowering the transformation temperature.

(5) Other advantages of the proposed process are its versatility, the ability to obtain high purity materials without large amounts of by-products without the need for washing, energy saving by using a low processing temperature, and the possibility to recycle the generated CO_2 and NH_3 gases to form the $(NH_4)_2CO_3$ reagent. It is also possible to use $NaAlO_2$ waste solution from dissolution of aluminium hydroxide or bauxite.

Conflicts of interest

There are no conflicts to declare.

Acknowledgements

This work was supported by the Scientific Grant Agency of the Ministry of Education of the Slovak Republic and the Slovak Academy of Sciences under contract VEGA 1/0176/19.

References

1 C. Liu, J. Li, K. Liew, J. Zhu and M. R. Bin Nordin, *RSC Adv.*, 2012, **2**, 8352–8358.
2 J. Wang, K. Shang, Y. Guo and W. C. Li, *Microporous Mesoporous Mater.*, 2013, **181**, 141–145.
3 G. Wu, G. Liu, X. Li, Z. Peng, Q. Zhou and T. Qi, *RSC Adv.*, 2019, **9**, 5628–5638.
4 R. Takahashi, A. Onishi, F. Sato and M. Kuramoto, *J. Ceram. Soc. Jpn.*, 2017, **125**, 742–746.
5 K. Zhang, Z. Fu, T. Nakayama, T. Suzuki, H. Suematsu and K. Niihara, *Mater. Res. Bull.*, 2011, **46**, 2155–2162.
6 T. F. Baumann, A. E. Gash, S. C. Chinn, A. M. Sawvel, R. S. Maxwell and J. H. Satcher Jr, *Chem. Mater.*, 2005, **17**, 395–401.
7 J. Y. Park, S. G. Oh, U. Paik and S. K. Moon, *Mater. Lett.*, 2002, **56**, 429–434.
8 R. López-Juárez, N. Razo-Perez, T. Pérez-Juache, O. Hernandez-Cristobal and S. Y. Reyes-López, *Results Phys.*, 2018, **11**, 1075–1079.
9 G. C. Li, Y. Q. Liu, L. L. Guan, X. F. Hu and C. G. Liu, *Mater. Res. Bull.*, 2012, **47**, 1073–1079.
10 T. E. Bell, J. M. Gonzáles-Carballo, R. P. Tooze and L. Torrente-Murciano, *RSC Adv.*, 2017, **7**, 22369–22377.
11 K. Ullmann, P. Ádám and K. Sinkó, *J. Non-Cryst. Solids*, 2018, **499**, 394–400.
12 L. Samain, A. Jaworski, M. Edén, D. M. Ladd, D. K. Seo, F. J. Garcia-Garcia and U. Häussermann, *J. Solid State Chem.*, 2014, **217**, 1–8.
13 A. R. Ferreira, E. Küçükbenli, A. A. Leitão and S. De Gironcoli, *Phys. Rev. B: Condens. Matter Mater. Phys.*, 2011, **84**(23), 235119.
14 D. C. Shin, S. S. Park, J. H. Kim, S. S. Hong, J. M. Park, S. H. Lee, D. S. Kim and G. D. Lee, *J. Ind. Eng. Chem.*, 2014, **20**, 1269–1275.
15 R. Rogojan, E. Andronescu, C. Ghitulică and B. S. Vasile, *U.P.B. Sci. Bull.*, 2011, **73**, 67.
16 A. Cheraitia, A. Ayral, A. Julbe, V. Rouessac and H. Satha, *J. Porous Mater.*, 2010, **17**, 259–263.
17 P. Pentyala, M. Shahid, S. Ramamirtham and M. G. Basavaraj, *Colloids Surf., A*, 2018, **544**, 172–178.
18 H. Kong, J. K. Lee and S. J. Lee, *J. Ceram. Process. Res.*, 2017, **18**, 726–730.
19 K. Roy, C. Jatejarungwong and P. Potiyaraj, *J. Appl. Polym. Sci.*, 2018, **135**, 46248–46256.
20 L. Lafficher, M. Digne, F. Salvatori, M. Boualleg, D. Colson and F. Puel, *Powder Technol.*, 2017, **320**, 565–573.
21 V. A. Matveev and D. V. Mairov, *Russ. J. Inorg. Chem.*, 2019, **64**(4), 438–444.
22 P. Wang, Z. D. Zhao, L. W. Bi, Y. X. Chen, L. Zhang and L. T. Sun, *Mater. Res. Innovations*, 2012, **16**(2), 121–125.
23 X. Hu, Y. Liu, Z. Tang, G. Li, R. Zhao and C. Liu, *Mater. Res. Bull.*, 2012, **47**(12), 4271–4277.
24 P. Billik and B. Horváth, *Inorg. Chem. Commun.*, 2008, **11**, 1125–1127.
25 G. R. Karagedov, *Chem. Sustainable Dev.*, 2011, **19**, 339–345.

26 G. R. Karagedov, S. S. Kosolobov, A. V. Latyshev, N. Z. Lyakhov and A. L. Myz, *Chem. Sustainable Dev.*, 2013, **21**, 603–608.
27 W. Wang, W. Liu, I. Y. Chang, L. A. Wills, L. N. Zakharov, S. W. Boettcher, P. H. Y. Cheong, C. Fang and D. A. Keszler, *Proc. Natl. Acad. Sci. U. S. A.*, 2013, **110**(46), 18397–18401, DOI: 10.1073/pnas.1315396110.
28 M. A. Hubbe, J. R. Metts, D. Hermosilla, M. A. Blanco, L. Yerushalmi, F. Haghighat, P. Lindholm-Lehto, Z. Khodaparast, M. Kamali and A. Elliott, *BioResources*, 2016, **11**(3), 7953–8091.
29 S. Abeysinghe, D. K. Unruh and T. Z. Forbes, *Cryst. Growth Des.*, 2012, **12**(4), 2044–2051.
30 C. V. Chandran, C. E. A. Kirschhock, S. Radhakrishnan, F. Taulelle, J. A. Martens and E. Breynaert, *Chem. Soc. Rev.*, 2019, **48**(1), 134–156, DOI: 10.1039/c8cs00321a.
31 T. Sato, S. Ikoma and F. Ozawa, *Thermochim. Acta*, 1984, **75**, 129–137.
32 M. Olszak-Humienik, *Thermochim. Acta*, 2001, **378**, 107–112.
33 A. Aghaeinejad-Meybodi, A. Ebadi, S. Shafiei, A. Khataee and A. D. Kiadehi, *Sep. Purif. Technol.*, 2019, **211**, 551–563.
34 Z. Zidi, M. Ltifi, Z. Ben Ayadi and L. El Mir, *J. Australas. Ceram. Soc.*, 2019, **7**(4), 524–535.
35 S. Ali, Y. Abbas, Z. Zuhra and I. S. Butler, *Nanoscale Adv.*, 2019, **1**, 213–218.
36 H. Koopi and F. Buazar, *Ceram. Int.*, 2018, **44**(8), 8940–8945.
37 T. F. Kemp and M. E. Smith, *Solid State Nucl. Magn. Reson.*, 2009, **35**(4), 243–252.
38 T. Shirai, H. Watanabe, M. Fuji and M. Takahashi, *J. Mater. Sci.*, 2009, **9**, 23–31.
39 Y. Li, J. Su and R. Li, *Microporous Mesoporous Mater.*, 2017, **243**, 9–15.
40 J. Landers, G. Y. Gor and V. Neimark, *Colloids Surf., A*, 2013, **437**, 3–32.
41 R. Laucournet, C. Pagnoux, T. Chartier and J. F. Baumard, *J. Am. Ceram. Soc.*, 2000, **83**(11), 2661–2667.
42 P. Persson, M. Karlsson and L. O. Öhman, *Geochim. Cosmochim. Acta*, 1998, **62**(23/24), 3657–3668.
43 A. R. Barron, *Dalton Trans.*, 2014, **43**, 8127–8143.
44 X. Wang, Ch. Li, Z. Shi, M. Zhi and Z. Hong, *RSC Adv.*, 2018, **8**, 8011–8020.
45 Y. Bang, S. J. Han, J. Yoo, J. H. Choi, J. K. Lee, J. H. Song, J. Lee and I. K. Song, *Appl. Catal., B*, 2014, **148–149**, 269–280.
46 S. Bi, C. Wang, Q. Cao and C. Zhang, *Coord. Chem. Rev.*, 2004, **248**, 441–455.
47 T. Sugimoto, *Monodispersed Particles*, Elsevier Science B.V., Amsterdam, 2001, pp. 273–275.
48 L. Zhang, X. Jiao, D. Chen and M. Jiao, *Eur. J. Inorg. Chem.*, 2011, **2011**(34), 5258–5264.
49 N. Nayak, N. Vitorino, J. R. Frade, A. V. Kovalenski, V. D. Alves, J. G. Grespo and C. A. M. Portugal, *Mater. Des.*, 2018, **157**, 119–129.